RSC Advances

PAPER

View Article Online
View Journal | View Issue

Cite this: *RSC Adv.*, 2020, **10**, 24265

Transport of nano zerovalent iron (nZVI) coupling with *Alcaligenes* sp. strain in porous media

Qing Xia, Mingzhu Huo, Peitong Hao, Junhao Zheng and Yi An *

Received 2nd March 2020
Accepted 18th June 2020

DOI: 10.1039/d0ra02004d

rsc.li/rsc-advances

Coupling nano zerovalent iron (nZVI) particles with anaerobic bacteria is a potentially powerful approach for remediating polluted groundwater. However, little is known about the transport of these mixed systems in porous media, which could potentially affect the system's activity and half-life in aqueous environments. This study assessed the transport and stability of nZVI coupled with *Alcaligenes* sp. TB by column experiments and sedimentation tests. The results showed that combined bio-nZVI systems experienced significantly higher transport and lower sedimentation rates than stand-alone nZVI. The transmission electron microscopy (TEM) and scanning electron microscopy (SEM) images showed that *Alcaligenes* sp. TB reduced aggregation of nZVI to some extent, though slight toxicity to bacteria was observed. The results of ζ-potential measurements demonstrated that the presence of bacteria increased the electrostatic force between the particles. Voltammetry, X-ray diffraction (XRD), and X-ray photoelectron spectroscopy (XPS) analysis confirmed that the bio-nZVI system undergoes different redox processes. The presence of bacteria favored the formation of FeOOH not Fe_2O_3 or Fe_3O_4, resulting in weaker surface magnetic properties.

1. Introduction

Owing to their high surface area and excellent chemical reactivity, nano zerovalent iron particles (nZVI) have gained widespread attention over the past decade for their high potential for treating groundwater pollution. Previous studies have shown that nZVI can be used to remediate groundwater and wastewater contaminated with nitrate,[1–3] azo dyes,[4,5] arsenic,[6,7] heavy metals (cadmium, lead, copper, chromium, nickel, zinc),[8–11] chlorinated organic compounds (COCs),[12–15] nitro-aromatic compounds (NACs),[16] phenol,[17] dissolved metals (CrO^{4-}, UO_2^{2+}, Cu^{2+}, Ni^{2+}, Pb^{2+}),[18,19] and other pollutants.[20]

When nZVI particles are applied for water treatment under continuous aerobic/anaerobic conditions, various bacterial communities, such as reductive dehalogenators and autotrophic denitrifiers that exist in the environment inevitably come into contact with nZVI either directly or indirectly.[21,22] Although many studies evaluating the toxicity of nZVI on bacterial have been conducted, hydrogen from nZVI corrosion may be the most significant benefit for many metabolic groups of these bacteria as a preferred electron donor. Therefore, in recent years, coupling nZVI with anaerobic bacteria appeared as one of the most promising methods in groundwater remediation. The combination of autotrophic bacteria with nZVI may provide an alternate method for the degradation of nitrate, as the hydrogen generated by anaerobic iron corrosion may stimulate denitrifying populations, making application more reliable[23] (eqn (1)).

$$Fe^0 + 2H_2O \rightarrow Fe^{2+} + H_2 + 2OH^- \quad (1)$$

Our previous studies[24–26] have shown that nZVI coupled with *A. eutrophus* for degrading nitrate can avoid the disadvantages of traditional biological denitrification, which depends on the use of explosive hydrogen. Moreover, the addition of autotrophic bacteria appeared to reduce the production of ammonium during treatment with nZVI; nitrate was completely removed by the bio-nZVI system with a lower proportion of resultant ammonium. Other studies have combined *Dehalococcoides* spp. with nZVI for the remediation of halogenated compounds.[27] Two main mechanisms were involved in this system, as both nZVI and *Dehalococcoides* spp. can simultaneously or sequentially degrade/remove pollutants, and *Dehalococcoides* may also be stimulated by corrosive H_2 as it is a preferable electron donor for its respiration.[28]

Although previous studies have shown that the bio-nZVI system enhanced the removal efficiency of pollutants, the transport of this system in the groundwater has received little attention. The high reactivity of nZVI alone is not sufficient to ensure effective remediation, and some important issues need to be addressed for successful full-scale applications. The key points are stability against aggregation, mobility in the underground environment, and longevity in underground conditions.[29] To be effective repair aquifers *in situ*, iron particles

Innovative Team of Monitoring and Precaution for Cropland Environment, Agro-Environmental Protection Institute, Tianjin, 300191, China. E-mail: simon8601@126.com

should remain in the suspension long enough to allow slurry preparation, handing, and injection underground. Moreover, they should have sufficient mobility underground to be transported around the injection point to some extent.[30] However, due to the van der Waals attractive force, electrostatic force as well as magnetic interactions, nZVI particles tend to aggregate rapidly into micro-scale, chain-like clusters.[31] Particle aggregation not only results in reduced chemical reactivity, but also reduces the ability of particles to transport in groundwater. The effect microorganisms exert on the transport of nZVI has not been addressed to date.

This study investigated the transport and stability of nZVI coupled with *Alcaligenes* sp. TB by column experiments and sedimentation tests. For a better understanding of the interaction mechanisms, representative samples were further investigated by transmission electron microscope (TEM), scanning electron microscopy (SEM), ζ-potential measurements, volt-ampere characteristic curve, X-ray diffraction (XRD) and X-ray photoelectron spectroscopy (XPS). To our knowledge, this is the first study to investigate the effect of anaerobic bacteria on the mobility of nZVI in porous media. Therefore, this study may help fill some of the knowledge gaps in the mobility of nano-iron in aquifers and the combined application of nano-iron and bacteria in groundwater remediation.

2. Material and methods

2.1 Preparation of combined bio-nZVI systems

Nano-iron particles were purchased from Hongwu Nano Materials (Guangzhou, China). The average particle size was ~50 nm and the specific surface area was 30–50 $m^2\ g^{-1}$.

Alcaligenes eutrophus was purchased from the China Center of Industrial Culture Collection (Beijing, China), and seed culturing and incubation protocols used in this study were similar to those described in our previous work.[32]

Combined bio-nZVI systems were prepared in 150 mL serum bottles. A certain amount of the *Alcaligenes eutrophus* cell suspension (20, 40, or 60 mL, with an optical density at 422 nm of about 0.07) was added to each bottle and then diluted to a total volume of 120 mL. The proportion of cell suspensions in the mixtures was 1/6, 1/3, and 1/2 (v/v ratio), respectively. Subsequently, the culture was purged with Ar gas for 20 min to remove residual oxygen, and then transferred into another deoxidized serum bottle containing 0.12 g of nZVI particles using the standard Schlenk and vacuum line techniques. The initial pH was adjusted to 7.0 with HCl (0.5 M). Bottles were sealed with Teflon septa and aluminum crimps, and mixed at 150 rpm using a rotary shaker at 30 °C. Parallel experiments were also performed without autotrophic bacteria.

2.2 Column transport experiments

Transport experiments were conducted in sand-packed columns (10 cm long and 2.2 cm i.d.). Columns were packed wet[33] with quartz sand ($d_{50} = 1140$ μm, coarse sand) as a model porous media. The average porosity of the packed column was determined gravimetrically to be 0.38. Nylon mesh (100 mm opening size) was placed at the bottom of the column to prevent sand leaking into the tube. Prior to being used, sand was acid-washed with concentrated HCl to remove minerals, then rinsed with deionized water and dried. Packed columns were flushed with at least 10 pore volumes (PV) of 1 mM $NaHCO_3$ solution to provide a uniform surface charge. The injection velocity of the nZVI suspension was maintained at 0.36 cm min^{-1} with a peristaltic pump, corresponding to injection conditions currently applied in field studies.[34] In each run, around 8 PVs of nZVI suspension (~1 g L^{-1} total iron) with different proportions of *A. eutrophus* were injected into the column; control injections of a pure nZVI suspension (~1 g L^{-1}) were performed in parallel. To prevent aggregation and sedimentation, the particle suspension was mixed at 300 rpm during injection. After injection, the column was flushed with 8 PV of deionized water to achieve complete breakthrough of the nanoparticles. Effluent samples were collected effluent samples were collected using a fraction collector for AAS analysis, and were dissolved in concentrated HCl (1 : 2 v/v ratio), diluted with 5% HNO_3, before being analyzed for total Fe at a wavelength of 249.7 nm. The breakthrough curve for each transport experiment was plotted as the normalized total Fe concentration (C/C_0) *versus* number of pore volumes. The presented data are the mean results from duplicate measurements.

2.3 Sedimentation experiments

The colloidal stability of nZVI particles in aqueous suspensions was evaluated by examining the sedimentation profile of the particle suspensions at pH 7. The sedimentation profiles were obtained by monitoring the optical density as a function of time. A UV-Vis spectrophotometer (UV-6100BS, Shanghai Media Corporation, China) was used for absorbance measurements of the supernatant in sealed cuvettes containing 1 g L^{-1} nZVI suspensions. The nZVI suspensions in the absence and presence of cell suspension were prepared and shaken without sonication before the experiment. All measurements were made at room temperature and all the experiments were run in triplicate.

2.4 nZVI characterization

The morphology and aggregation states of the nZVI nanoparticles were analyzed using TEM (Zeiss sigma 300, Germany) operating at 200 kV. The morphology of the bacterial strains incubated with 1 g L^{-1} of nZVI for 1 h were examined by scanning electron microscopy (SEM) and transmission electron microscopy (TEM), using standard procedures for fixing and embedding sensitive biological samples.[35]

ζ-Potential measurements were carried out with a zeta-potential analyzer (Zetasizer Nano ZS90). The measurements were carried out with nZVI suspension at 25 °C. Averaged values were obtained from three measurements.

Volt-ampere characteristic curves were acquired to determine the effect of bacteria on nZVI redox processes, measured using an electrochemical workstation with a sensitivity of 100 μA operating at an initial potential of −1.2 V for a scan speed of 0.05 V s^{-1}.

The oxidation products of nZVI were examined by XRD (Ultima IV, X'Pert PRO MPD) at 40 kV and 30 mA. The nZVI particles were scanned from 20° to 90°, which covered all major iron and iron oxides.[36]

The XPS spectra of the nanoparticles were determined by using an ESCALAB 250Xi technique employing an MgK_{α} source. The binding energies of the photoelectrons were calibrated by the aliphatic adventitious hydrocarbon C(1s) peak at 284.80 eV.

3. Results and discussion

3.1 Characterization of nZVI and microorganisms

The morphologies of the nZVI, identified from TEM images, are shown in Fig. 1, in which the individual particles appeared to be spherical, with the presence of an oxide shell of ~5 nm of thickness stabilizing the core of the particles; this is consistent with results described in other publications.[37] All particles were aggregated and form chain-like clusters due to both their magnetic properties and their tendency to remain in the most thermodynamically favorable state[38] (Fig. 1a). With the addition of *A. eutrophus*, a more stable suspension of nZVI was attained. The TEM images showed that the bacteria served an agent preventing nZVI from the aggregation to some extent, as the clusters formed in the presence of *A. eutrophus* showed looser structures than those of bare nZVI (Fig. 1b).

Particular attentions should be given to structural and functional changes induced by nanomaterials in bacterial cell. The first goal of the nanostructures is to attach to the surface of the bacterial cell wall, which involves a large number of molecular interactions.[39] These interactions can cause structural, morphological changes and damage, and even cell death in some cases.[40] In this work, SEM analysis was conducted using bacterial samples with and without the presence of nZVI. The image (Fig. 1e) illustrated the morphologies of cells in the absence of nZVI, and they are of a moderately sized bacilliform shape. SEM images showed that the presence of nZVI around some bacteria, although they did not cause obvious changes in cell morphology. When exposed to nZVI (Fig. 1f), it was observed that the nZVI layer adhered to the cell membrane, although it did not cause a significant change in the bacterial cell morphology. The molecular and cellular interaction between nZVI and bacterial cells was evaluated by TEM (Fig. 1c).

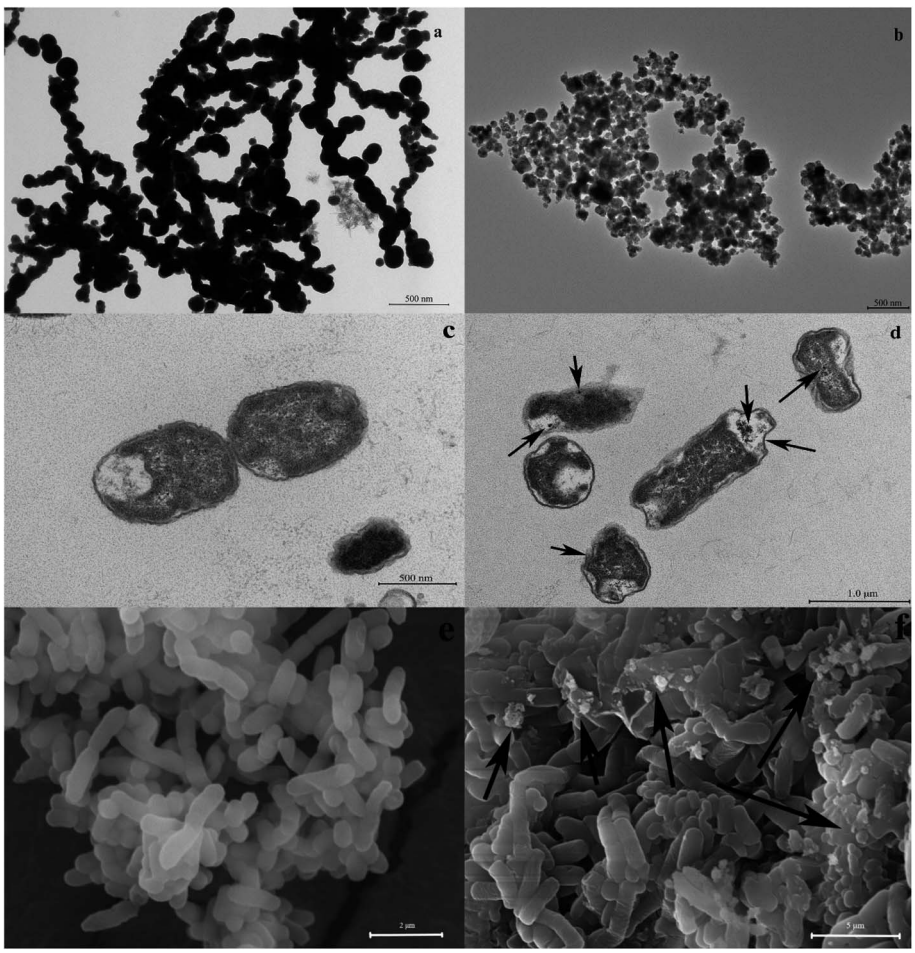

Fig. 1 (a) TEM images of nZVI alone; (b) TEM images of bio-nZVI system; (c) TEM images of non-treated *A. eutrophus* cells; (d) TEM images of *A. eutrophus* treated with 1 g L^{-1} nZVI for 60 min; (e) SEM image of non-treated *A. eutrophus* cells; (f) SEM image of *A. eutrophus* treated with 1 g L^{-1} nZVI for 60 min.

In the absence of nanoparticles, TEM images showed clear cell walls and uniformly stained cell interiors, corresponding to the proteins and DNA. In the treated cells, TEM micrographs confirmed that nZVI associated to cells caused deformation of the cellular wall even penetrated a percentage of the cells (Fig. 1d).

3.2 Breakthrough curves of the bio-nZVI suspension

Understanding nZVI transport is critical to assessing the migration potential of nZVI from the injection point to the target environmental site. In groundwater remediation applications, nZVI is typically directly injected at concentrations on the order of 10 g L^{-1},[41,42] although concentrations as low as 0.75–1.5 g L^{-1} (ref. 43) and as high as 50 g L^{-1} (ref. 44) have been used. Here, a single concentration of nZVI particles (1 g L^{-1}) was used. Column transport experiments were conducted using bio-nZVI suspensions with cell suspension ratios of 1/6, 1/3, and 1/2 (v/v ratio). The effluent was collected every 2 min using an automatic fraction collector.

Fig. 2 presented the breakthrough curves of column experiments for bio-nZVI suspensions and bare nZVI. For the test of bare nZVI, the results show that the relative concentration (C/C_0) in the effluent for the bare-nZVI is no more than 0.1 over 8 PV, indicating that these particles were immobile. In contrast, the nanoparticles displayed relatively superior mobility in the presence of *A. eutrophus* cells. In all cases, the nanoparticle breakthrough started at ~2 PV, and then rose sharply to a steady full breakthrough concentration plateau at ~3 PV. The steady-state relative (C/C_0) for the bio-nZVI systems with 1/6, 1/3, and 1/2 (v/v ratio) cell suspension were 0.2, 0.3, and 0.4, respectively. The transportation of the bio-nZVI system was considerably better in comparison to the bare nZVI suspension, and as the proportion of *A. eutrophus* cells increased, the transportability increased as well. Although the presence of *A. eutrophus* was shown to improve the transport of nZVI particles in porous media, high retention was still observed, likely due to the formation of large aggregates over time. Such a small fraction of nanoparticles at the outlet points out that further stabilization is needed to enhance their mobility.

After completing the injection of nZVI at 8 PV, deionized water was pumped into the column to flush the nZVI deposited in the column. Except for a small peak at 10 PV with 1/6 (v/v ratio) cell suspension, the concentration of nZVI dropped sharply without tailing, indicating that the release of nanoparticles from the sand was negligible.[45] This irreversible deposition could be of great practical significance, as indicates that the nanoparticles released underground can be expected to remain in a confined area. The split peak may be attributed to some large nZVI that migrated slowly in the column and was flushed out by DI water.[46]

Transportability of nanoparticles in the porous media was mainly dependent on stability of the suspension and particle charge. The bare nZVI particles showed very poor mobility when injected into porous media; the retention of the unstable nZVI suspension is likely due to the large particle aggregates, formed due to the attractions between the particles.[33] As shown in Fig. 1a, bare nZVI aggregated and formed chain-like clusters. With the addition of cell suspension, a more stable suspension of nZVI can be attained (Fig. 1b). The clusters formed in the presence of *A. eutrophus* showed looser structure than bare nZVI cluster structures. Stability of nZVI suspensions was further tested by sedimentation experiments.

3.3 Stability of bio-nZVI suspension

The extent of colloidal stability of nZVI suspensions with different proportions of *A. eutrophus* cell suspension (0, 1/6, 1/3, and 1/2, v/v ratio) was qualitatively measured by sedimentation tests. In the sedimentation tests, the absorbance at 508 nm of nanoparticles suspensions was recorded every 5 minutes and the results are shown in Fig. 3. A decrease in absorbance over time occurred because of the reduction in the number of particles in the suspension due to aggregation, as well as the settlement out of solution over time of heavier aggregates.

It was observed that nZVI sedimentation was slowest at proportion of 1/2 (more than 45% of nZVI particles remained in

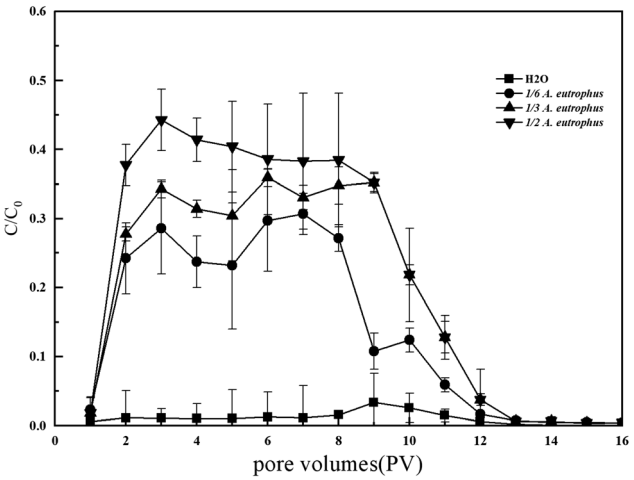

Fig. 2 Comparison of breakthrough curves of bio-nZVI suspension.

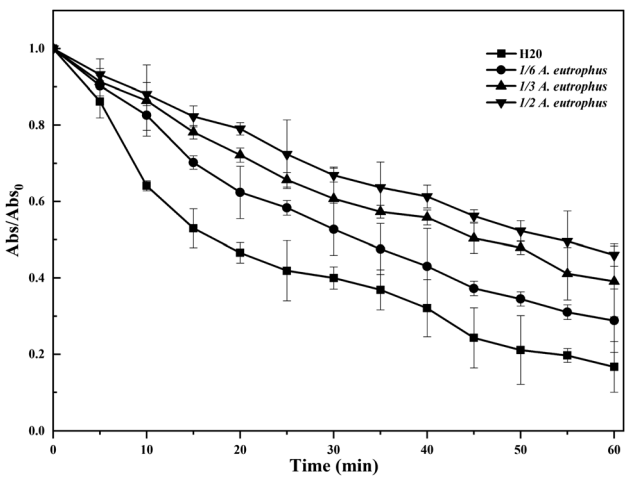

Fig. 3 Colloidal stability assessed through sedimentation tests of nZVI.

suspension at the end of the experiment), considerably faster at 1/3 and 1/6 nZVI (around 40%, 31% of particles remained in the suspension at the end of the experiment), and the highest with bare nZVI (only around 10% of particles remained in the suspension after the experiment). These results indicated that nZVI sedimentation proceeded much slower in the presence of *A. eutrophus*.

Previous study has revealed that a rapid sedimentation often occur when the size of aggregates reach a critical size (d_c). Settlement of nZVI may follow two processes: (1) direct sedimentation of some particles with larger size ($d > d_c$), and (2) aggregation of the residual particles with smaller size ($d < d_c$) followed by sedimentation.[47] As demonstrated in Fig. 3, the deposition rate was low in the first ten minutes, and the particles agglomerated to form chain aggregates. Between 10–30 minutes, sedimentation becomes rapid where the chain-like aggregates reached a critical size. After 40 minutes, the sedimentation rate once again became low, potentially due to the deposition of aggregates that did not form chain clusters of critical size.[31] The aggregation is closely related to the surface charge of the nanoparticles, in which the lower the surface charge, the lower electrostatic repulsion among the particles, and thus the more aggregation. The dispersion of the nZVI particles in the presence of *A. eutrophus* could be ascribed to enhancing the electrostatic repulsion effect. Hence, the ζ-potential analysis of nZVI in the presence of *A. eutrophus* was carried out. The ζ-potential indicates the extent of the electrostatic interactions between nanoparticles. The results showed that for bare-nZVI the ζ-potential is nearly zero (-1.38 ± 1.13) and logically the electrostatic repulsion is also small. After adding *A. eutrophus*, the ζ-potentials was -23.1 ± 1.6. The presence of bacteria increased the absolute value of ζ-potential of iron nanoparticles, thereby increasing the electrostatic force between the particles. What's more, aquifer materials generally have universal negative surface charges in the neutral pH range.[48] Thus, the repulsive force between iron nanoparticles and aquifer materials also increased, which promoted their stability in porous media.

In this study, it can be speculated that the enhanced of nZVI stability was also can attributed to changes in the corrosion products of nZVI, which then affect the magnetic interactions between nZVI particles. To confirm this, the volt-ampere characteristic curves, XRD, and XPS were used.

3.4 Volt-ampere characteristic curve analysis of two systems

nZVI particles are unstable in aquifers, and a series of corrosion reactions may occur. Aqueous Fe^0 corrosion generally occurs through an electrochemical mechanism (Fig. 4). The anode process is the dissolution of Fe^0, while the cathode is a process in which hydrogen is released as a gas under anaerobic conditions, following eqn (1). The Fe^{2+} may hydrolyze and form Fe $(OH)_2$ on the surface of Fe^0 (eqn (2)). Ferrous (Fe^{2+}) and trivalent iron (Fe^{3+}), which are known to have cytotoxic effects, are first released near the surface of the nanoparticles and gradually oxidized to form Fe(II) and Fe(III) oxides. Study indicated that the rod-shaped bacteria, *e.g.*, *Acidithiobacillus ferrooxidans*,

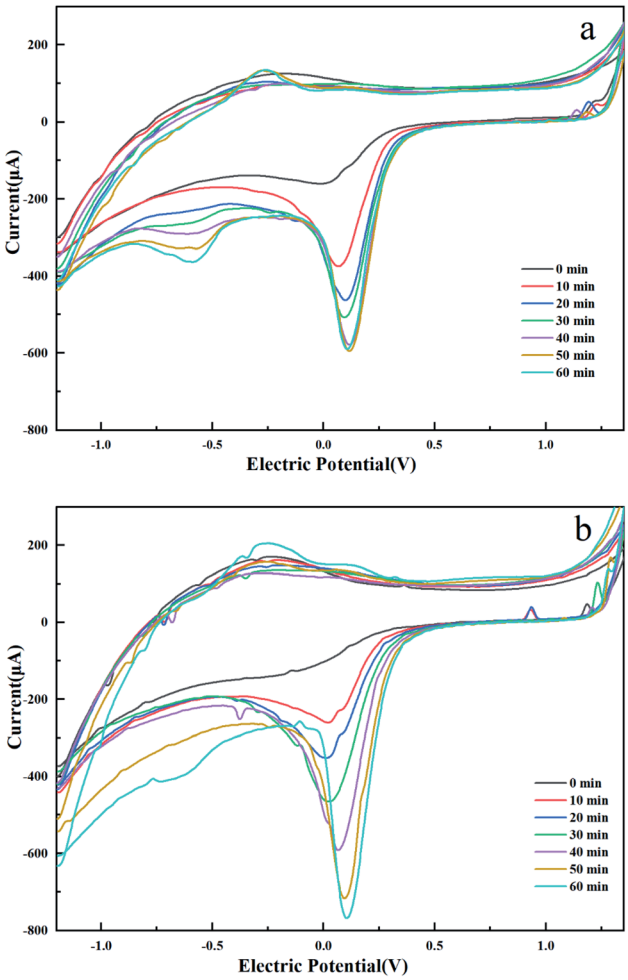

Fig. 4 Volt-ampere characteristic curves of (a) nZVI and (b) bio-nZVI system.

mediated rapid oxidization of the Fe^{2+} to Fe^{3+}.[49] Because Fe^{2+} and Fe^{3+} are only stable in certain environments, they temporarily exist in the environment, but eventually oxidize to insoluble iron, such as Fe_2O_3, Fe_3O_4, FeOOH (eqn (3)–(6)).[50] High oxidation rates will favor the formation of lepidocrocite (FeOOH) (eqn (5) and (6)).[51] The different current and redox potential between the two systems examined indicated that the bacteria accelerated nZVI corrosion in water (Fig. 4). Studies have shown that anionic structures such as those of *B. subtilis* walls promote ferric hydroxide formation.[52,53] It was observed that iron preferentially adhered to the cell wall of *B. subtilis*, which caused the walls to adhere together, forming iron oxyhydroxides to form macroscopic flocs.[52] These were identical to what was observed in this work. As different iron corrosion products may be generated in each system, the X-ray diffraction (XRD) spectrum and XPS technology were used to further verify the difference in the iron corrosion products between these two systems.

$$Fe^{2+} + 2H_2O \rightarrow Fe(OH)_2 + 2H^+ \quad (2)$$

$$2Fe^{2+} + 3H_2O \rightarrow \gamma\text{-}Fe_2O_3 \quad (3)$$

$$6Fe^{2+} + O_2 + 6H_2O \rightarrow 2Fe_3O_4 \quad (4)$$

$$4Fe^{2+} + O_2 + 6H_2O \rightarrow 4\gamma\text{-FeOOH} \quad (5)$$

$$4Fe_3O_4 + O_2 + 6H_2O \rightarrow 12\gamma\text{-FeOOH} \quad (6)$$

3.5 The XRD and XPS analysis of two systems

The composition evolution of the nZVI and bio-nZVI systems was investigated by XRD analysis, which clearly illustrated that the chemical composition differed between the two systems. The peaks at 33, 57 and 75° were credited to maghemite (Fe_2O_3) or magnetite (Fe_3O_4) nZVI corrosion products[54] (Fig. 5a). There was an obvious peak at 44–45°, indicating the presence of Fe^0 in the bio-nZVI system[55] (Fig. 5b); this may indicated that the corrosion products of nZVI in the bioreactor being amorphous. XPS technology was used to verify the iron corrosion products in the bio-nZVI systems.

The XPS survey scans for the bare nZVI system and the bio-nZVI system are show in Fig. 6, with Fig. 6a showing the XPS spectrum in the Fe 2p region of the nZVI in the integrated system. In the inserted Fe 2p high-resolution scan, the

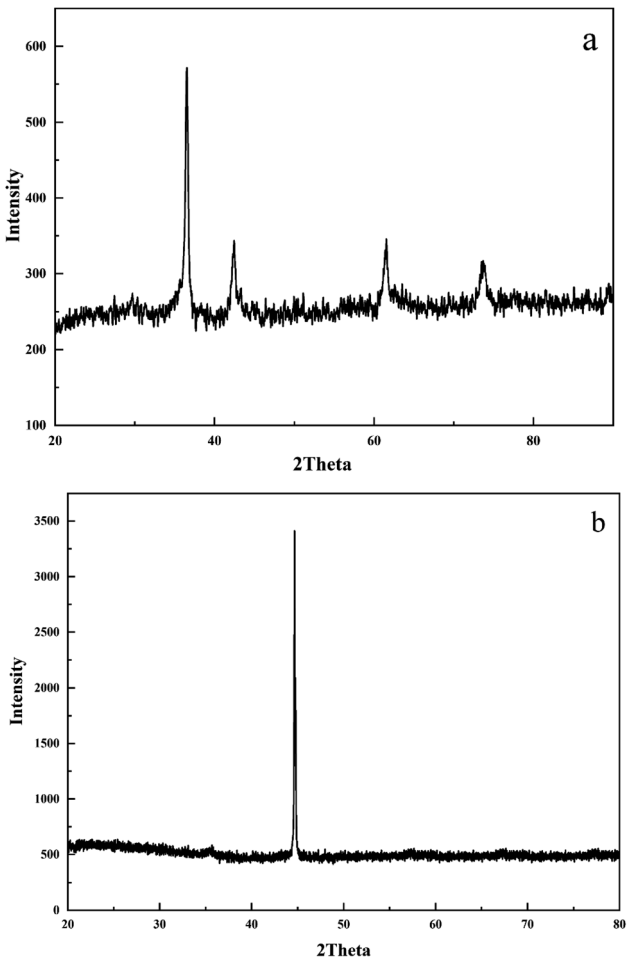

Fig. 5 XRD profiles of (a) nZVI alone and (b) bio-nZVI system.

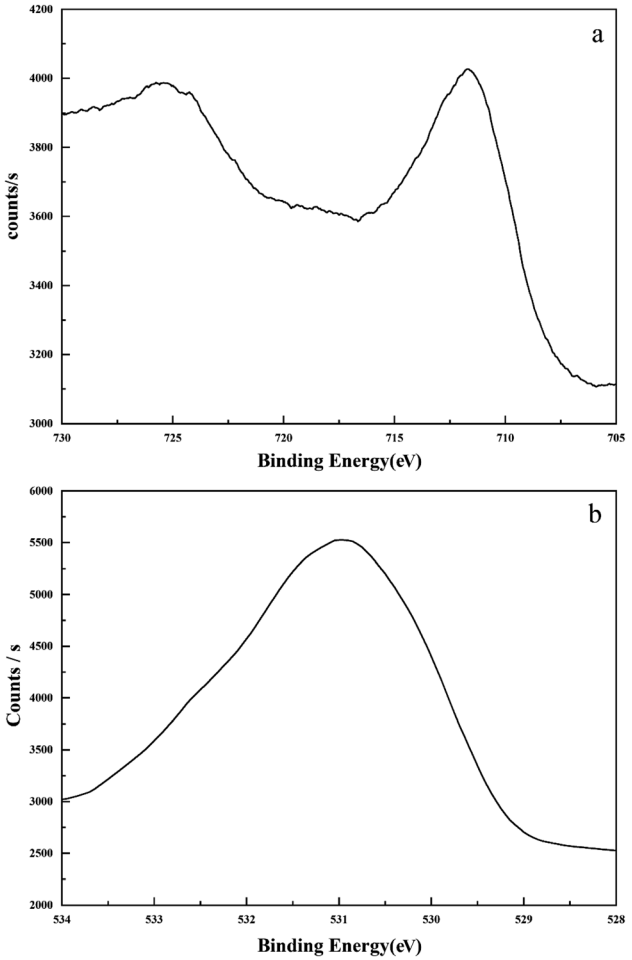

Fig. 6 XPS survey of (a) Fe 2p and (b) O 1s of nZVI in the presence of *A. eutrophus*.

characteristic peaks at 711.2 and 724.9 eV representing $2p_{3/2}$ were present, and the binding energies of the satellites $2p_{3/2}$ and $2p_{1/2}$ were shown, suggesting the presence of Fe(III) oxides, which was in accordance with the results of XRD. Since Fe_2O_3 and FeOOH have similar characteristics and peak positions, an investigational scan of O 1s was also performed to observe the surface oxygen state (Fig. 6b). The O 1s was decomposed into three components: (i) oxygen-formed ionic bond, O^{2-}, at 529.9 eV; (ii) oxygen double bonded with carbon or phosphorus from carboxylic acids, carboxylates, esters, carbonyls, amides, or phosphoryl groups, at 531.4 eV; and (iii) oxygen attributable to hydroxide, phosphate, acetal, or hemiacetal, C–OH, C–O–C and P–OH, at 530.5 eV.[56] A single peak at 531 eV was observed, representing an OH group; these results indicate that iron oxide may be in the FeOOH state rather than the Fe_2O_3 state in the bio-nZVI system.

Kielemoes *et al.* demonstrated that the addition of micro-organisms can improve the performance of iron corrosion and hydrogen production, and also demonstrated that the addition of microorganisms can change the reaction selectivity of zero-valent iron.[57] This could be because certain enzymes in bacteria (*e.g.* [Fe]-Hase) can catalyze the reduction of protons to

hydrogen, which may enhance the transport of electrons from the nZVI to water;[58] however, no data was obtained in this study to support this hypothesis. It has been suggested that presence of FeOOH species at the surface of nZVI particles weakens their surface magnetic properties.[59,60] As discussed earlier, the extent of aggregation of nZVI is mainly controlled by magnetic, van der Waals, electrostatic and steric forces between particles; as a result, formation of FeOOH may result in disruption to the magnetic attraction between nZVI particles. Because of this, the stability of the nZVI suspension was improved, which resulted in enhanced transport in porous media.

4. Conclusion

This study investigated the transport and stability of the bio-nZVI system by column experiments and sedimentation tests. Although slight toxicity to bacteria was observed, the presence of *A. eutrophus* was found to enhance the transport and stability of nZVI suspensions. The presence of bacteria increased the absolute value of ζ-potential of iron nanoparticles, thereby increasing the electrostatic force between the particles. Voltammetry, XRD, and XPS analysis confirmed that the bio-nZVI system undergoing different redox processes. The presence of bacteria favored the formation of FeOOH not Fe_2O_3 or Fe_3O_4, resulting in weaker surface magnetic properties. Although the presence of *A. eutrophus* improved the transport of nZVI particles in porous media, the results are still not ideal. New strategies will therefore be required in order to improve bio-nZVI system transport in porous media. One strategy towards this aim is using a combination of anaerobic bacteria and polyelectrolyte-modified nZVI particles. The introduced polyelectrolyte coatings can promote the stability of nZVI suspensions as well as bacterial growth in the subsurface, as previously demonstrated by Johnson *et al.*[61,62] It also should be noted that the present study was performed with a pure hydrogenotrophic culture of *Alcaligenes eutrophus*; in order to more closely replicate *in situ* conditions, the results obtained here need to be verified using a mixed culture in future study.

Conflicts of interest

There are no conflicts to declare.

Acknowledgements

This work was funded by the National Natural Science Foundation of China (grant no. 41203082 & 41573107) and the Municipal Key Program of Natural Science Foundation of Tianjin (grant no. 14JCZDJC40700).

References

1 Y. H. Hwang, D. G. Kim and H. S. Shin, *J. Hazard. Mater.*, 2011, **185**, 1513–1521.
2 A. Ryu, S. W. Jeong, A. Jang and H. Choi, *Appl. Catal., B*, 2011, **105**, 128–135.
3 J. Zhenmao, L. Lu, Z. Weiming, D. Qiong, P. Bingcai, Y. Lei and Z. Quanxing, *Water Res.*, 2011, **45**, 2191–2198.
4 S. Salma and V. K. Balakrishnan, *Environ. Sci. Technol.*, 2011, **45**, 10369–10377.
5 S. Luo, P. Qin, J. Shao, L. Peng, Q. Zeng and J.-D. Gu, *Chem. Eng. J.*, 2013, **223**, 1–7.
6 N. Anke, K. Ralf, V. Andreas, H. Abul, A. K. M. Munir and S. J. Hug, *Environ. Sci. Technol.*, 2013, **47**, 4544–4554.
7 S. Klas and D. W. Kirk, *J. Hazard. Mater.*, 2013, **252–253**, 77–82.
8 S. Li, W. Wang, F. Liang and W. X. Zhang, *J. Hazard. Mater.*, 2017, **322**, 163–171.
9 C. Ding, W. Cheng, Y. Sun and X. Wang, *Geochim. Cosmochim. Acta*, 2015, **165**, 86–107.
10 W. F. Chen, J. Zhang, X. Zhang, W. Wang and Y. Li, *Environ. Sci. Pollut. Res. Int.*, 2016, **23**, 1460–1470.
11 Y. Su, A. S. Adeleye, Y. Huang, X. Zhou, A. A. Keller and Y. Zhang, *Sci. Rep.*, 2016, **6**, 26918.
12 F. Fu, D. D. Dionysiou and H. Liu, *J. Hazard. Mater.*, 2014, **267**, 194–205.
13 S. Chunming, R. W. Puls, T. A. Krug, M. T. Watling, S. K. O'Hara, J. W. Quinn and N. E. Ruiz, *Water Res.*, 2012, **46**, 5071–5084.
14 L. M. Kustov, E. D. Finashina, E. V. Shuvalova, O. P. Tkachenko and O. A. Kirichenko, *Environ. Int.*, 2011, **37**, 1044–1052.
15 K. Choi and W. Lee, *J. Hazard. Mater.*, 2012, **211–212**, 146–153.
16 W. Yin, J. Wu, P. Li, G. Lin, X. Wang, B. Zhu and B. Yang, *Chem. Eng. J.*, 2012, **210**, 309–315.
17 A. Shimizu, M. Tokumura, K. Nakajima and Y. Kawase, *J. Hazard. Mater.*, 2012, **201**, 60–67.
18 T. Liu, X. Yang, Z. L. Wang and X. Yan, *Water Res.*, 2013, **47**, 6691–6700.
19 L. Z. Zhang, Y. Mu, F. Jia and Z. Ai, *Environ. Sci.: Nano*, 2016, **4**, 27–45.
20 D. O'Carroll, B. Sleep, M. Krol, H. Boparai and C. Kocur, *Adv. Water Resour.*, 2013, **51**, 104–122.
21 T. D. Hang, J. Kuever, M. Mussmann, A. W. Hassel and F. Widdel, *Nature*, 2004, **427**, 829–832.
22 M. L. Kalmokoff and K. F. Jarrell, *Can. J. Microbiol.*, 2011, **34**, 557–576.
23 Y. Liu and G. V. Lowry, *Environ. Sci. Technol.*, 2006, **40**, 6085–6090.
24 Y. An, T. Li, Z. Jin, M. Dong, Q. Li and S. Wang, *Sci. Total Environ.*, 2009, **407**, 5465–5470.
25 Y. An, Q. Dong and K. Zhang, *Chemosphere*, 2013, **103**, 86–91.
26 A. Yi, T. Li, Z. Jin, M. Dong, H. Xia and X. Wang, *Bioresour. Technol.*, 2010, **101**, 9825–9828.
27 Z. M. Xiu, K. B. Gregory, G. V. Lowry and P. J. J. Alvarez, *Environ. Sci. Technol.*, 2010, **44**, 7647–7651.
28 C. D. T. F. Aulenta, C. Cupo, M. Petrangeli Papini and M. Majone, *J. Chem. Technol. Biotechnol.*, 2006, **81**, 1520–1529.
29 T. Tosco, M. Coisson, D. Xue and R. Sethi, *Zerovalent iron nanoparticles for groundwater remediation: Surface and magnetic properties, colloidal stability, and perspectives for*

field application, Research Signpost, Kerala, 2012, pp. 201–223.
30 S. R. Kanel, D. Nepal, B. Manning and H. Choi, *J. Nanopart. Res.*, 2007, **9**, 725–735.
31 T. Phenrat, N. Saleh, K. Sirk, R. D. Tilton and G. V. Lowry, *Environ. Sci. Technol.*, 2007, **41**, 284–290.
32 C. Xu, X. Wang, Y. An, J. Yue and R. Zhang, *Chemosphere*, 2018, **202**, 644–650.
33 N. Saleh, K. Sirk, Y. Liu, T. Phenrat, B. Dufour, K. Matyjaszewski, R. D. Tilton and G. V. Lowry, *Environ. Eng. Sci.*, 2007, **24**, 45–57.
34 T. Phenrat, H.-J. Kim, F. Fagerlund, T. Illangasekare and G. V. Lowry, *J. Contam. Hydrol.*, 2010, **118**, 152–164.
35 I. Sondi and B. Salopek-Sondi, *J. Colloid Interface Sci.*, 2004, 177–182.
36 Y. P. Sun, X. Q. Li, J. Cao, W. X. Zhang and H. P. Wang, *Adv. Colloid Interface Sci.*, 2006, **120**, 47–56.
37 B. Schrick, B. W. Hydutsky, J. L. Blough and T. E. Mallouk, *Chem. Mater.*, 2004, **16**, 2187–2193.
38 Y. H. Lin, H.-H. Tseng, M.-Y. Wey and M.-D. Lin, *Sci. Total Environ.*, 2010, **408**, 2260–2267.
39 A. E. Nel, L. Mädler, D. Velegol, T. Xia, E. M. V. Hoek, P. Somasundaran, F. Klaessig, V. Castranova and M. Thompson, *Nat. Mater.*, 2009, **8**, 543–557.
40 J. Díaz-Visurraga, A. García and G. Cárdenas, *J. Appl. Microbiol.*, 2010, **108**, 633–646.
41 N. Saleh, H. J. Kim, T. Phenrat, K. Matyjaszewski and G. V. Lowry, *Environ. Sci. Technol.*, 2008, **42**, 3349–3355.
42 K. M. Sirk, N. B. Saleh, T. Phenrat, H. J. Kim and R. D. Tilton, *Environ. Sci. Technol.*, 2009, **43**, 3803–3808.
43 D. W. Elliott and W.-x. Zhang, *Environ. Sci. Technol.*, 2001, **35**, 4922–4926.
44 N. C. Mueller, J. Braun, J. Bruns, M. Černík, P. Rissing, D. Rickerby and B. Nowack, *Environ. Sci. Pollut. Res.*, 2012, **19**, 550–558.
45 Y. L. Y. Wang, J. D. Fortner, J. B. Hughes, L. M. Abriola and K. D. Pennell, *Environ. Sci. Technol.*, 2008, **42**, 3588–3594.
46 P. Jiemvarangkul, W. X. Zhang and H. L. Lien, *Chem. Eng. J.*, 2011, **170**, 482–491.
47 H. Dong, K. Ahmad, G. Zeng, Z. Li, G. Chen, Q. He, Y. Xie, Y. Wu, F. Zhao and Y. Zeng, *Environ. Pollut.*, 2016, **211**, 363–369.
48 Y. P. Sun, X.-q. Li, J. Cao, W.-x. Zhang and H. P. Wang, *Adv. Colloid Interface Sci.*, 2006, **120**, 47–56.
49 B. Jones and R. W. Renaut, *Sediment. Geol.*, 2007, **194**, 77–98.
50 E. Lefevre, N. Bossa, M. R. Wiesner and C. K. Gunsch, *Sci. Total Environ.*, 2016, **565**, 889–901.
51 N. Kumar, M. Auffan, J. Gattacceca, J. Rose, L. Olivi, D. Borschneck, P. Kvapil, M. Jublot, D. Kaifas and L. Malleret, *Environ. Sci. Technol.*, 2014, **48**, 13888–13894.
52 I. T. Mayers and T. J. Beveridge, *Can. J. Microbiol.*, 1990, **35**, 764–770.
53 S. G. Walker, C. A. Flemming, F. G. Ferris, T. J. Beveridge and G. W. Bailey, *Appl. Environ. Microbiol.*, 1989, **55**, 2976–2984.
54 A. Liu, J. Liu, J. Han and W. X. Zhang, *J. Hazard. Mater.*, 2017, **322**, 129–135.
55 X. Q. Li and W. X. Zhang, *Langmuir*, 2006, **22**, 4638–4642.
56 Y. Lv, Z. Niu, Y. Chen and Y. Hu, *Water Res.*, 2017, **115**, 297–308.
57 J. Kielemoes, P. De Boever and W. Verstraete, *Environ. Sci. Technol.*, 2000, **34**, 663–671.
58 J. A. Wright, P. J. Turrell and C. J. Pickett, *Organometallics*, 2010, **29**, 6146–6156.
59 K. Naresh, A. Mélanie, G. JérôMe, R. JérôMe, O. Luca, B. Daniel, K. Petr, J. Michael, K. Delphine and M. Laure, *Environ. Sci. Technol.*, 2014, **48**, 13888–13894.
60 Y.-S. Li, J. S. Church and A. L. Woodhead, *J. Magn. Magn. Mater.*, 2012, **324**, 1543–1550.
61 H. J. Kim, T. Phenrat, R. D. Tilton and G. V. Lowry, *J. Colloid Interface Sci.*, 2012, **370**, 1–10.
62 R. L. Johnson, G. O. B. Johnson, J. T. Nurmi and P. G. Tratnyek, *Environ. Sci. Technol.*, 2009, **43**, 5455–5460.